COMPRESSION AFTER IMPACT (CAI) PROPERTIES OF CF/PEEK (APC-2) AND CONVENTIONAL CF/EPOXY STIFFENED PANELS

Takashi Ishikawa, Yoichi Hayashi and Masamichi Matsushima

Airframe Division, National Aerospace Laboratory
6-13-1, Ohsawa, Mitaka-shi, Tokyo 181, JAPAN

ABSTRACT

Compression after impact (CAI) tests are conducted for stiffened panels as main components of aircraft wing structure. Difference of the delamination buckling behavior during CAI tests due to the material is compared in detail. Improvement of CAI strengths by AS4/PEEK(APC-2) over CF/Epoxy is demonstrated. Before CAI testing, impact damages are given by a drop weight impact analyzer and delamination area is measured by a robotic ultrasonic NDI system. Relationships between impact energy and delamination area are obtained. Level-off in the area for CF/Epoxy is related to the change of damage mode; from delamination to penetration. Final failure process in CAI tests is well described by a plenty of data of 50ch. strain, Moire-topography pictures, and multi-channel AE analyzer. Path of delamination propagation in the CF/Epoxy specimens is captured. In the CF/PEEK specimens, delamination propagation is well arrested just by the instance of catastrophic failure, and hence, high CAI strengths are obtained. CAI strength of CF/PEEK with the best quality (FY89) is improved 37% to that of CF/Epoxy. Finite element analysis is conducted for obtaining a better correlation between prediction and experiments for linear buckling behavior. Effects of material nonlinearity and model geometry are clarified.

1. INTRODUCTION

Weight reduction is the most important goal in the design of aerospace structures. Current reduction ratios of approximately 20% to metal structures by an employment of conventional carbon/epoxy composites, however, are not fully satisfactory figure if we consider very high strengths of recent carbon fibers. Some part of the reason of the less reduction ratio could be ascribed to poor fracture toughness of such carbon/epoxy composites. A low level of allowable strain for a CAI strength[1] is one typical example of the criticality caused by the poor toughness. Therefore, a strong expectation for tough composites is now arising in the aerospace composite society. Carbon fiber(CF)/thermoplastic composites, particularly CF/PEEK system, are capable candidate materials[2] for satisfying such a requirement. Some preliminary data[3] implies that CF/PEEK show an excellent CAI result. Because CAI properties are the major reason for the reduction of design allowable strains, it can be expected that larger strain space will be allowed in the design and that higher ratio of weight reduction will be brought by an employment of CF/PEEK.

A practical research program of 6 years is now undergoing in NAL of JAPAN in order to verify and examine the weight reduction of aircraft wing structure by CF/PEEK. A fabrication of wing structure models of AS4/APC-2 and an evaluation of their performance are the final goals of the program. In-house fabrication of coupon level specimens in NAL[2] was done precedently to those of complicated specimens conducted by Fuji Heavy Industries Co.LTD (FHI). The CAI tests for flat plates made of CF/PEEK and CF/epoxy are performed first through NASA method. The CAI tests for stiffened panels are then performed and reported here. Numerical analysis by FEA is pursued in order to provide physical understanding of linear and nonlinear behavior of buckling problems of stiffened panels. Testing of semi-span wing model, the final part of the program, will be carried out in the near future.

2. SUMMARY OF CAI RESULTS FOR THICK PLATES

CAI tests can be regarded as a suitable measure of damage tolerance characteristics of composites. The essence of the preceding CAI results[4] done for thick plates through NASA method[5] is described below. A comparatively thick quasi-isotropic plate with stacking sequence of 48 plies:$[(45/0/-45/90)^6/_{sym.}]$ is used for CF/PEEK and CF/epoxy material systems. As the CF/Epoxy material, AS/410 resin system of Mitsubishi Rayon Co. is employed because plenty of basic material data are available. Chosen CF/PEEK material here is AS4/APC-2 by Fiberite Corp. Averaged thickness of the plates is 7.3mm for CF/Epoxy and 6.2mm for CF/PEEK, respectively.

Impacts of about 27 Joule, about 4kJ/m in normalized expression by thickness, are applied to the plates by an instrumented drop-weight type impactor, Dynatup GRC8250 system. This machine is the same one as used in the panel tests and explained later. Compression tests are conducted by an Instron 1128 screw-driven testing machine for the plates after or before impact. The loaded and supported ends are almost clamped and the side edges are almost simply supported.

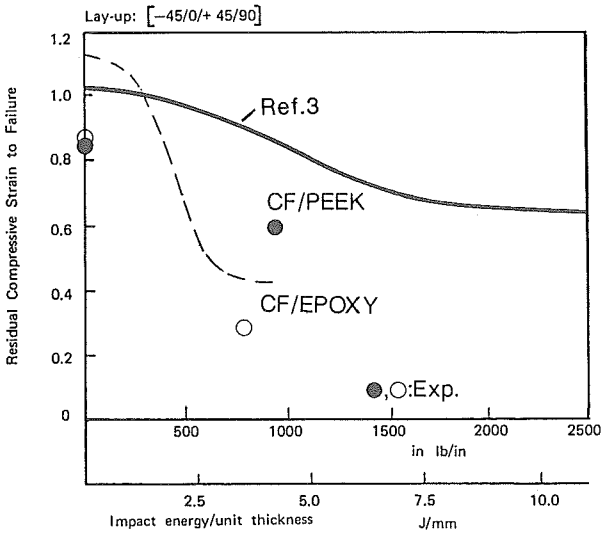

Figure 1 Relationships between CAI Strains and Normalized Impact Energy by Thickness for NASA type Plates

As a summary of these tests, CAI strengths are plotted in Fig.1 as the function of the normalized impact energy by the thickness. It can be understood that CAI strengths of flat plates of CF/PEEK is almost twice of those of CF/Epoxy plates. Moire-topography pictures showing delamination propagation pattern for both composite systems are depicted in Fig.2 where percentages indicate the ratios of the current loading to the maximum. Pictures for CF/Epoxy imply that delamination penetrates easily through the specimen across the loading direction. This behavior gives an basis of comparison with the following stiffened panel results.

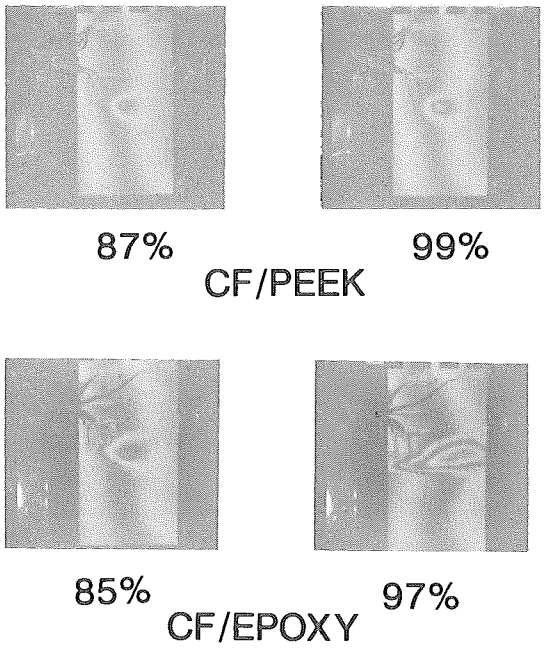

Figure 2 Moire-Topography Pictures of Plates Taken at the Indicated Relative Loadings

3. CAI TESTS OF STIFFENED PANELS

Stiffened panel is one of the most important structural concepts in aircraft wing and fuselage. Therefore, it is required to compare CAI behavior of stiffened panels[6] and the aforementioned thick plates. Although current process technology is matured enough for CF/Epoxy panel, a fabrication work of CF/PEEK panel is far beyond daily technique. It took four years and plenty of money to raise the processing technology of CF/PEEK up to the level of CF/ Epoxy.

Dimensions and typical stacking sequence of the test pieces are depicted in Fig.3. The commonness in both material panels is maintained as far as possible. However, there exist some distinctions in the detailed specifications like stacking sequence and bonding technology. Descriptions and classifications of the test panels are listed in Table 1. The detail of stacking sequence is listed in Table 2. CF/Epoxy panels are cut out from a wing box model subjected to a static test[7] and used as second-hand after a strict ultrasonic inspection. This situation is the reason why the fabrication year of the CF/Epoxy articles is old. Their stacking sequence was so designed as to satisfy the requirement of the strength of the model. The sequence of CF/PEEK is determined to follow the predecessor as much as possible. In FY86 Specimens of CF/PEEK, there exist three major different points from others because of poor processing technology: Shape of the stiffener is L instead of T, the stacking sequence is completely different, and fusion bonding is not applied. The quality is getting better as later fabrication years. Aluminum end fixtures are glued to the panel with potting material. Effects of potting and fixture upon buckling stresses will be discussed later.

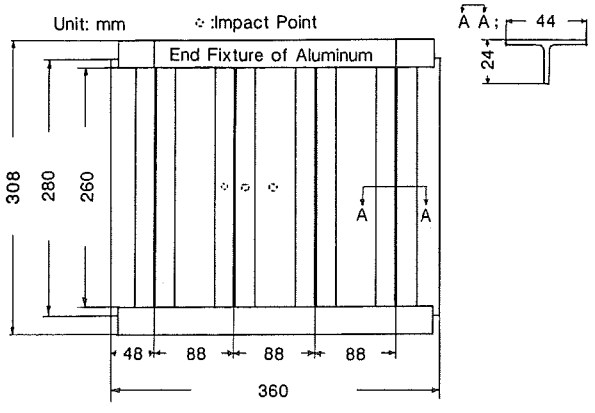

Stacking Sequence in CFRP Panels (s.:Symmetric)

	Stiffeners	Skin
CF/PEEK(FY89)	: (45/-45/-45/45/0^4/90/0^3)s.	(45/-45/-45/45/0/90)s.
CF/Epoxy	: (±45f/0/0:90f/0^2)s. f;fabric	(45/-45/45/-45/90)s.

Figure 3 Dimensions and Stacking Sequence of Stiffened Panels of Both Material Systems

Table 1 Descriptions of Stiffened Panel Specimens

Material	CF/Epoxy (S410)	CF/PEEK (APC-2)		
Specimen ID	CE 01 02 03 04 05 06 07 08	CPFY86 01 02 03 04	CPFY88 01 02 03 04	PEH 01 02
Impact Location[#]	/ CB SC SC S S S S°	/ CB / /	/ SC S S	/ S
Nrm. Impact Engy. (kJ/m)	8.2 8.2 3.0 4.0 8.2 2.0 4.0	8.2	8.2 4.0 8.2	4.0
Fabrication Year	FY82	FY86	FY88	FY89
Stiffener Shape	T	L	T	T
Bonding Method[&]	ML	AH	FB	FB
Stacking Sequence[$]	F	B	A	AA
Quality	Excellent	Poor-Fair	Good	Excl.

[#]: / =No Impact, CB=Central Bay on Skin, SC=on Stiffener and CB, S=on Stiffener (Inner Bay), S°=on Stiffener (Outer Bay)
[&]: ML=Monolithic, AH=Bonded with Epoxy Adhesive, FB=Fusion Bonded with PEEK Film
[$]: Stacking Sequence is indicated in Figure 7.

Table 2 Detail of Stacking Sequence

Specimen Group ID	Stacking Sequence in Stiffener (Web)	Stacking Sequence in Skin
CE	$(\pm 45_{fabric}/\ 0/0:90_{fabric}/0^2)_{sym.}$	$(45/\ -45/\ 45/\ -45/\ 90)_{sym.}$
CPFY86	$(45/\ 0^2/\ -45/\ 0^2/\ 45/\ 0/\ -45/\ 90)_{sym.}$	$(45/\ -45/\ 45/\ -45/\ 90)_{sym.}$
CPFY88	$(45/\ -45/\ -45/\ 45/\ 0^3/\ 90/\ 0^2)_{sym.}$	$(45/\ -45/\ -45/\ 45/\ 90)_{sym.}$
PEH	$(45/\ -45/\ -45/\ 45/\ 0^4/\ 90/\ 0^3)_{sym.}$	$(45/\ -45/\ -45/\ 45/\ 0/\ 90)_{sym.}$

Impacts are applied by the same drop-weight impactor as used in the plate tests. A picture around the impact head of 12.7mm diameter is shown in Fig.4.

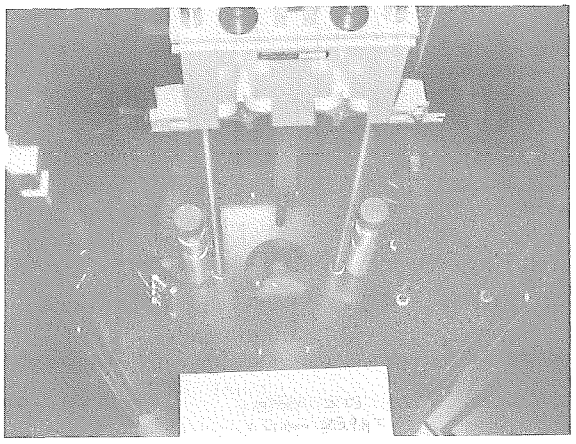

Figure 4 Picture of Impact Test: Impact Head of Dynatup GRC 8250 System. [Panel is placed underneath a bed.]

Impact locations are diversified from the skin at the middle bay (CB) to the center of the stiffener flange, (S) and (S°). Three panels have dual impacts for checking their effect. Normalized impact energy by the thickness of impacted points varies in the range from 2.0 to 8.2 kJ/m.

The impacted panels are subjected to ultrasonic inspection by a robotic C-scan system newly introduced in NAL by Krautkramer Japan Co. LTD. This system has an extraordinary accuracy and versatility for a larger size and shapes of objects. Some examples of delamination C-scope at stiffeners of CF/Epoxy panels with different impact energy are depicted in Fig. 5. Projection areas of delamination are measured from such outputs. Relationships between the areas and normalized energy are shown in Fig.6 for both material panels. It is clearly understood that the relationship is almost proportional to impact energy in full range for CF/PEEK and

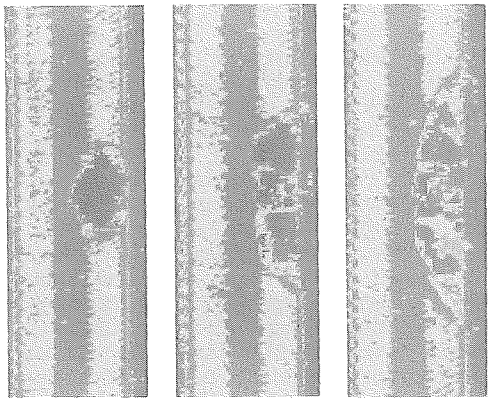

Figure 5 Examples of Delamination C-Scope under Various Relative Impact Energy for CF/Epoxy panels

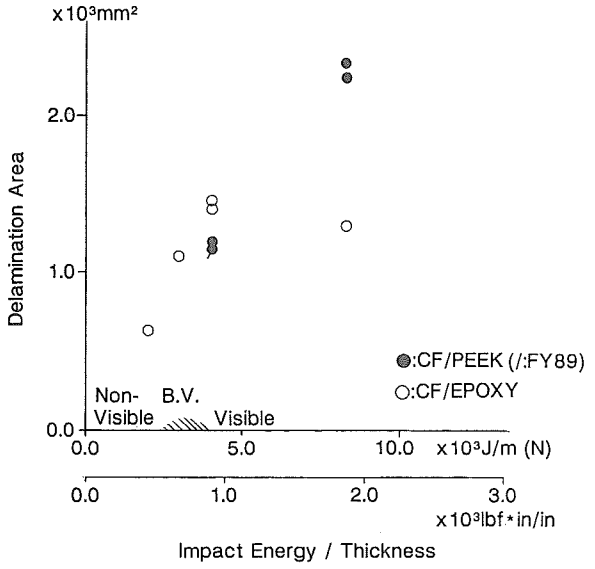

Figure 6 Relationships between Delamination Area and Normalized Impact Energy for Panels

that it is also linear up to 4 kJ/m despite levelling off over this value for CF/Epoxy. Ultrasonic and visual observation reveals that impact damage mode in CF/Epoxy changes from delamination to penetration over this levelling off value.

Compression tests are conducted by the same Instron 1128 machine as stated earlier with a cross head speed of 0.2mm/min. Loading ends with bonded fixtures and side edges can be approximately considered as fixed and simply supported, respectively. Data acquisition is performed per one second by HP-3852A system for 50 channels of strain, 6 channels of deflection and a channel of load. A testing setup is shown in Fig.7. Again, a Moire-topography camera is used for detecting buckling deformation.

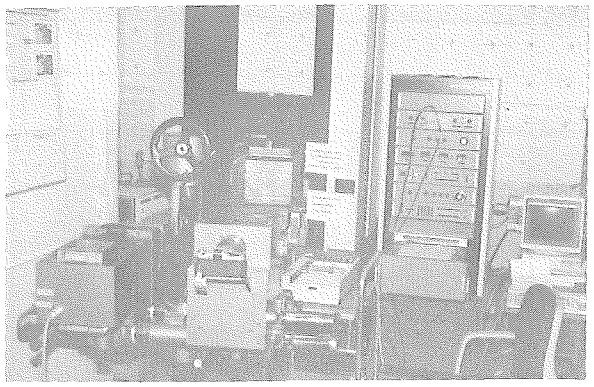

Figure 7 Setup of Testing Machine and Data Acquisition System

4. DISCUSSION ABOUT EXPERIMENTAL RESULTS OF STIFFENED PANELS

In order to simplify the discussion, summarizing results about CAI strengths of the panels are shown first in Fig. 8. Indication is done for an averaged value if there are multiple panels for the same group. Figure 8 shows variation of CAI strengths caused by specimen quality and impact location. Blank, hatched sparsely, hatched densely and filled columns correspond to CF/Epoxy (CE), CF/PEEK of FY86 (CPFY86), CF/PEEK of FY88 (CPFY88), and CF/PEEK of FY89 (PEH), respectively.

The first point of discussion about the results of Fig.8 is the effect of impact location. It is clearly shown that the present level impacts on skin at the center of the bay do not affect the compressive strength at all. There could be two reasons of such insensitivity to impacts: One reason is less axial stiffness of skin of the present panel due to the present stacking sequence, $[(45/-45/45/-45/90)_{sym.}]$ than the well-known results by NASA[8]. The other reason is that the present buckling stresses of skin-stiffener flange is rather lower than the corresponding values in the same reference. On the other hand, the present 4kJ/m impacts on the flange center of the stiffener degrade the strength seriously such as 34% in CF/Epoxy and 19% in CF/PEEK (CPFY88). This tendency implies that the stiffeners carry much more axial load than skin. Even in CF/Epoxy, however, it should be noted that a reduction ratio of CAI strength is not so severe as 60% in the thick plate cases. This fact will be mentioned later at a chance of discussion of individual results.

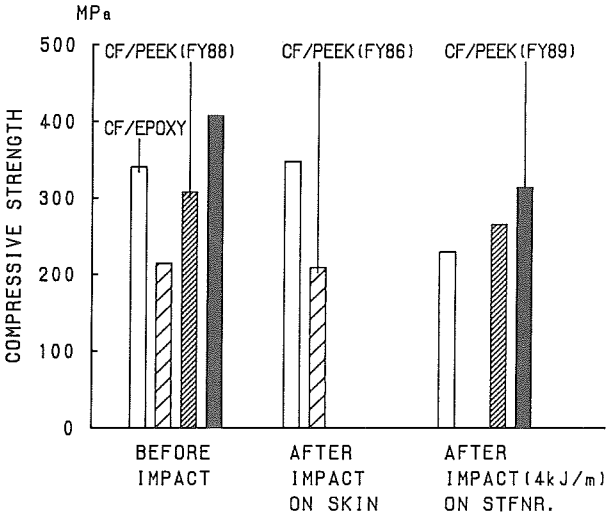

Figure 8 Summary of CAI Strengths for Stiffened Panels Based on Specimen Groups and Impact location

The second point of discussion in Figure 8 is the effect of the quality of the panels including the variety in stacking sequence. At the stage before impact, CPFY86 Specimens exhibit strength of 63% of CE specimens before impact. The reason can be ascribed to the stacking sequence of the stiffeners of CPFY86 panels indicated in Table 2. Figure 9 demonstrates the experimental and analytical results of

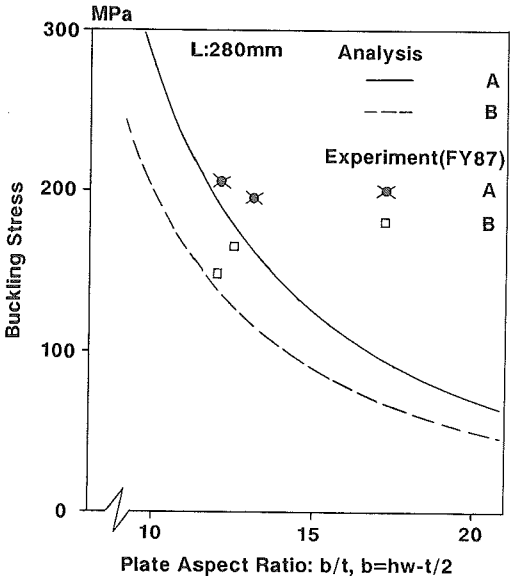

Figure 9 Difference of Buckling Stress by Stacking Sequence in T-Stiffener Web

preliminary compression tests of T-stiffeners themselves for 2 kinds of sequence[4]. Legends A and B denote the stacking sequences identical to CPFY88 and CPFY86, respectively. The method of analysis is similar to Ref.9 and stated later. Larger bending-twisting coupling terms, D_{16} and D_{26}, of Sequence B than A give approximately 30% reduction in buckling stress for the present b/t ratio of stiffener web. Such a low buckling stress leads to a poor compressive strength. Some additional reasons like immature processing technology and L-shape of stiffener can also affect the low compressive strength of CPFY86.

A considerable improvement in strengths can be achieved in CF/PEEK panels of PEH and CPFY88. CAI results of PEH and CPFY88 are about 37% and 10% better than the average of CF/Epoxy data, respectively. It should be noted that the quality of CPFY88 is inferior to the level of CF/Epoxy according to the robotic ultrasonic NDI. NDI indication reveals that a quality of PEH panels is almost reaching the same level of CE panels. Because before-impact strength of PEH is also a little larger than that of CF/Epoxy due to the difference of stacking sequence, some part of a 37% improvement in CAI strength of PEH to CE can be attributed to such a laminate design.

Variation of CAI strengths as a function of normalized impact energy by the thickness at an impact spot are shown in Fig.10 where the results of CPFY86 are omitted in plotting. The results of the plate shown in Fig.1 is again given for convenience sake. Even a slight impact could reduce compressive strength seriously in CF/Epoxy panel results indicated by open circles. However, as mentioned earlier, reduction ratio is smaller than the plate results indicated by open squares. Note that CF/PEEK (CPFY88) results indicated by filled circles without slash exhibit insensitivity to impact apparently. The true reason might be ascribed to the low before-impact strength obtained for one of this group of panels. Its ultrasonic inspection with some defects during processing justifies such a presumption.

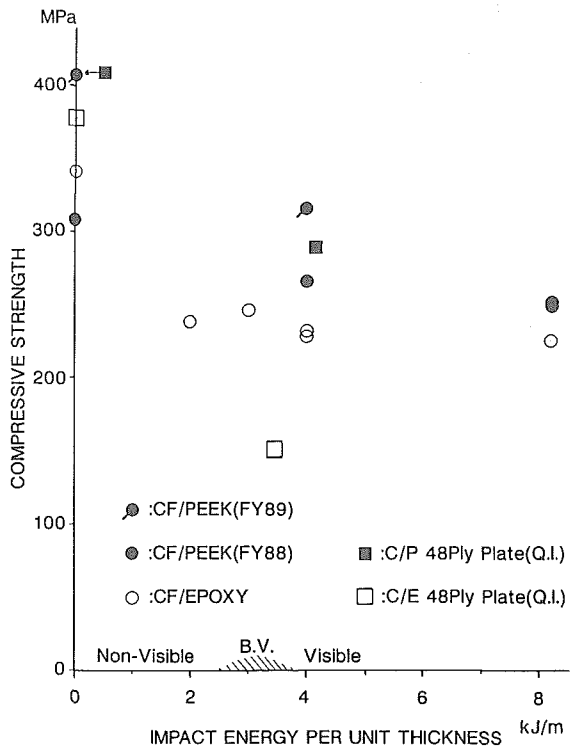

Figure 10 Relationships between CAI Strengths and Normalized Impact Energy for Stiffened Panels

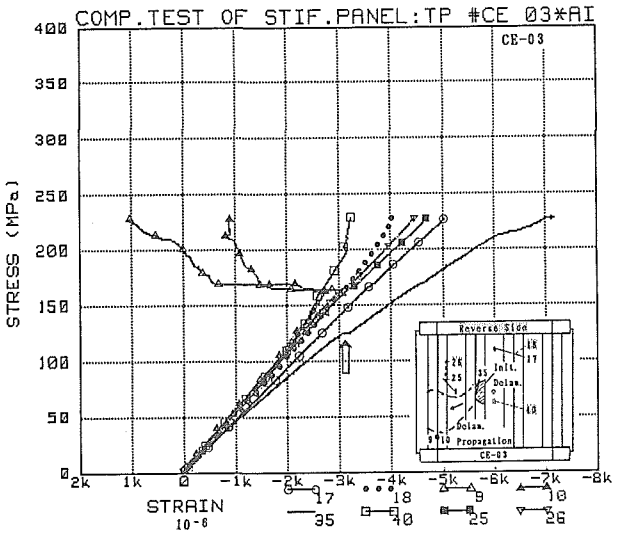

Figure 11 Stress-Strain Relations for CF/Epoxy (CE-03) Panel after Impact

From now on, individual test data will be discussed. The primary interest is the CAI behavior of CF/Epoxy panel (CE-03). Figure 11 shows stress vs. selected strain curves. A small leap in strain #35 at 125MPa indicated by a blank arrow and a rapid deviation in strains #9 and #10 from linear behavior over 160MPa can be identified. These sudden variation in behavior occur at 0.3% strain correspondingly with the CAI strain of thick plates. Stress-deflection relations are shown in Fig.12 where a small leap in #4 is observed. Taking the Moire-topography pictures into account, it is understood that there happens a quick delamination growth toward the lower left direction indicated in Figs. 11 and 12. The position of #4 sensor is located in the area of propagated delamination. Buckling of a mid-bay panel, skin and stiffener flange, might be a trigger of such a quick propagation. Some increase in load carrying capacity after the damage growth is observed in the stiffened panel in contrast with the cases of thick plates.

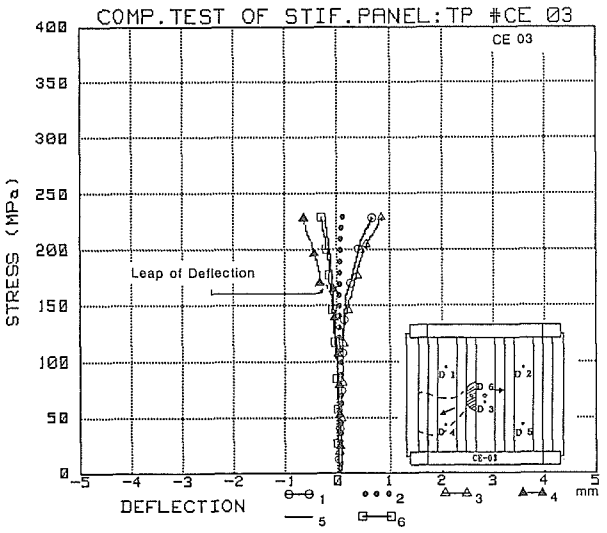

Figure 12 Stress-Deflection Relations for CE-03 after Impact

Contrary to this case, there is almost no arresting of delamination in CF/Epoxy thick plates once it starts propagating. Thus, it can be considered that the stiffened panel structure has a nature to localize the delamination. In other words, this type of a bay-by-bay panel exhibits a sort of the fail-safe capability similarly to fatigue crack propagation.

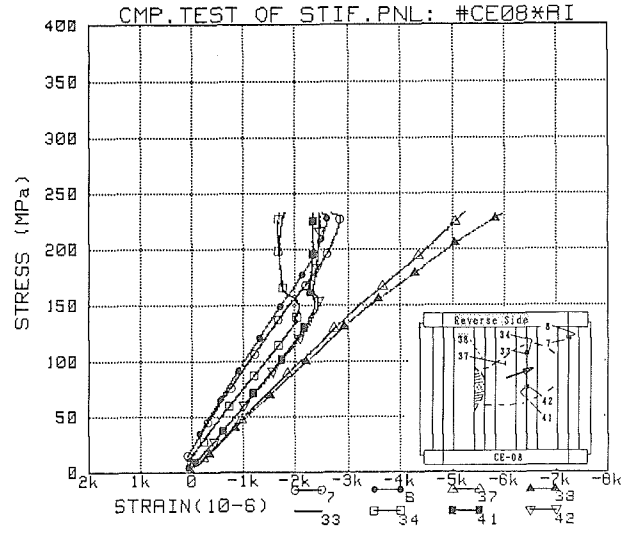

Figure 13 Stress-Strain Relations for CF/Epoxy (CE-08) Panel after Impact

Another CF/Epoxy CAI result for panel CE-08 is shown in Fig.13. Although impact level is the same as CE-03, 4kJ/m, the location of impact is different. In CE-03, the impact point is on the stiffener flange at the central bay, whereas it is on the flange at the left bay in CE-08. Delamination area caused by impact is indicated by hatching in Fig.13. Stress-strain relations demonstrate again that some deviation from common linear behavior takes place around 0.3% strain, CAI strain of conventional CF/Epoxy, and that the panel can carry more load. Such tendency in the behavior is quite similar to CE-03. CAI strength is about 230MPa and also pretty close to the value of CE-03. Moire-topography pictures indicate the delamination propagation direction upper right, reversely of CE-03. Such a direction reversal is natural if we consider a position of initial delamination.

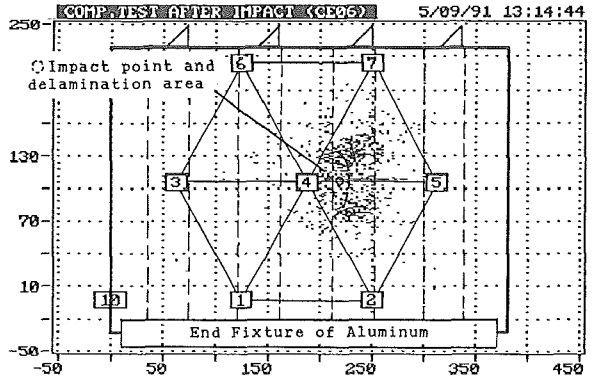

Figure 14 Results of Location Identification of AE sources by Multi-Channel AE Analyzer

Delamination propagation is also traced by acoustic emission (AE) technique. Used multi-channel AE system, SPARTAN AT by PAC Corp., has a capability to identify the location of AE source. Although the present skin exhibits slight anisotropy in AE wave velocity, the software based on isotropic velocity is utilized. A typical result of AE location identification is shown in Fig.14 for another CF/Epoxy panel, CE-06, with 3kJ/m impact on stiffener. Because this sketch of the panel is drawn from the skin side, right and left are opposite to those of sub-illustrations in Figs.11 to 13. Therefore, a location of impact and delamination shape are similar to those of CE-03. Figures in squares in Fig.14 denote ID number of AE sensors and dots indicate the identified location of AE sources. Thus, both propagation directions, upper right and lower right, can be identified from this figure. Such observation is consistent with findings from consecutive Moire-topography pictures.

Similar stress-strain relations for a CAI test of CF/PEEK Panel (PEH-02) and related Moire-topography pictures are shown in Figs.15 and 16. Given impact is again 4kJ/m. From Fig.15 and stress-deflection relations, initial buckling stress is determined as 230MPa. Local deflection around delamination starts roughly 70MPa earlier. The local deformation pattern can be identified at the location indicated by 4 arrows in Fig.16 (a). This picture is taken just before a delamination propagation mentioned later. With some increase of loading after the buckling, sudden delamination propagation

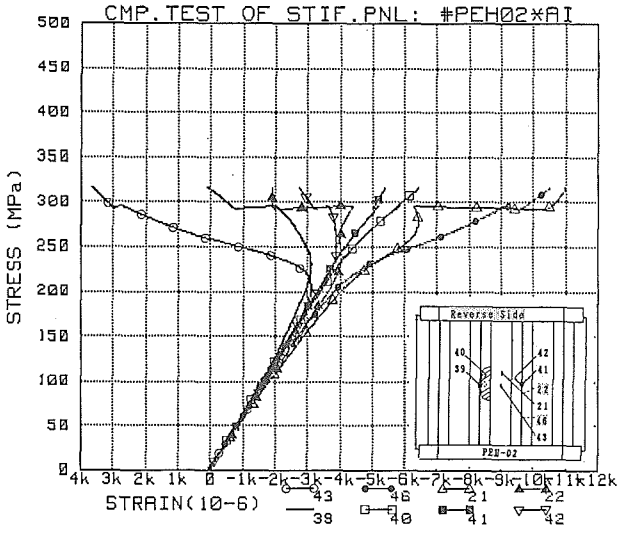

Figure 15 Stress-Strain Relations for CF/PEEK (PEH-02) Panel after Impact

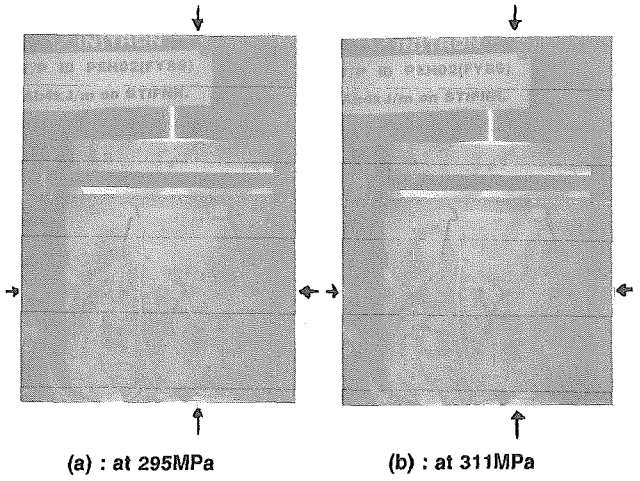

Figure 16 Moire-Topography Pictures in CAI Test of CF/PEEK Panel (PEH-02)

occurs nearby central AE sensor indicated by 4 arrows in Fig.16(b) at 296MPa. More increase of loading is possible, and finally, it fails at 314MPa. Hence, an ability of delamination arrest in CF/PEEK is ensured also in the stiffened panel. Note that some local compression strains exceed 1%. Thus, high CAI strength of CF/PEEK plotted in Fig.8 is obtained. However, the difference in CAI strengths of panels between CF/PEEK and CF/Epoxy is less enhanced than thick plates mainly due to the aforementioned intrinsic fail-safe characteristics in CF/Epoxy panels.

Some discussions about the behavior of panels of both material systems before impact will be given below. Stress vs. lateral deflection relations for showing an inter-bay buckling of a CF/Epoxy panel

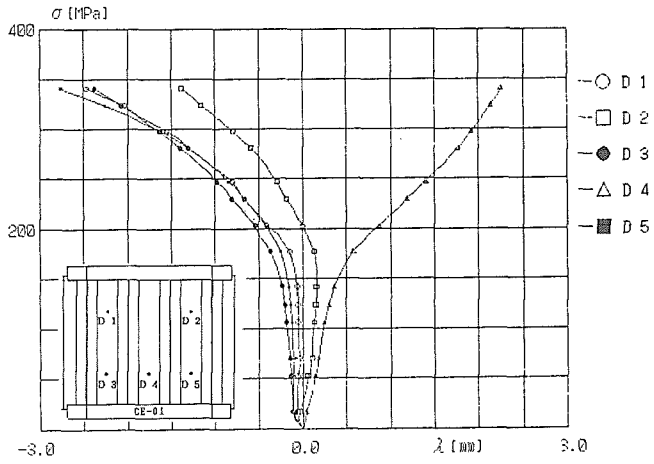

Figure 17 Stress-Deflection Relations for CE-01 before Impact

(CE-01) are given in Fig.17. The buckling stress is determined as 180 MPa by δ^2 method. Just before the final failure, a crippling occurs on stiffeners near end fixtures. Compressive strength reaches 341MPa which is close to a compressive strength before impact of a 48ply plate.

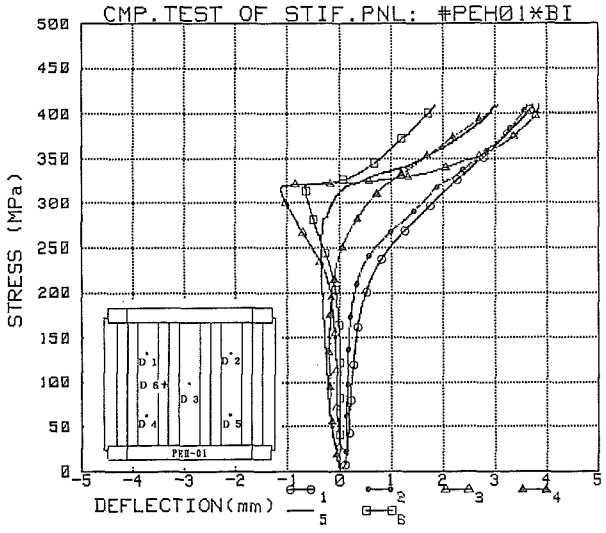

Figure 18 Stress-Deflection Relations for PEH-01 before Impact

Similar stress-lateral deflection relations of CF/PEEK (PEH-01) are shown in Fig.18. Moire-topography pictures will appear in the next section for comparison with the theory. There is a slight difference in deflection pick-up points. From this chart and omitted stress-strain relations, initial buckling stress is determined as 220MPa. A secondary buckling stress mainly in stiffener is estimated as 320MPa. This value is close to the crippling stress found in CE-01 before impact panel of CF/Epoxy. Finally, it fails catastrophically at 407MPa. This level of stress can be considered excellent as for rather thin stiffened panels.

5. BUCKLING ANALYSIS AND COMPARISON WITH EXPERIMENTAL RESULTS

5.1 GENERAL

Some buckling and postbuckling work has already been conducted for composite stiffened panels, e.g. Ref.8. Other literature, Refs.10-12 can be also found. Reference 8 gives the first extensive scope of compression after impact (CAI) properties of stiffened panels. However, even for initial buckling behavior, levels of agreement between theory and experiment are not fully satisfactory.

In this section, a better correlation is pursued. Theoretical tools used here are a finite element software package, NISA-II, and a common type of Rayleigh-Ritz method. The main reason of previous worse correlation[8] can be ascribed to the reducing longitudinal elastic modulus of unidirectional CFRP in compression. Because of a shorter configuration of the present stiffened panels, boundary conditions along the loading edges play a much more important role than in the previous cases. Effects of initial imperfection are also demonstrated quantitatively.

It is well-known that unidirectional CFRP exhibits dependency of longitudinal elastic modulus on stress levels. The authors once proposed a fractional constitutive relation[13] based on tensile tests of UD-CFRP. This equation is rewritten here:

$$E_L = 1 / (S_{11} + 2\, S_{111}\, \sigma_1 + 3\, S_{1111}\, \sigma_1^2) \qquad 1)$$

where E_L and σ_1 denote the longitudinal elastic modulus and stress, respectively. S_{11} is a common elastic compliance in the longitudinal direction, i.e., $S_{11} = 1/E_L$ in the pure linear case. S_{111} and S_{1111} denote the higher order elastic compliances. The best fit combination of S_{11}, etc. are determined in Ref.13 only by the tensile tests. Therefore, compression tests for measuring E_L are performed for CF/PEEK UD material in Ref.14. Obtained data of the longitudinal modulus are shown in Fig.19 with the previous data[13] for the same material. Then, S_{11}, etc. are estimated and Eq.1 is rewritten as follows for GPa unit:

$$E_L = 1000/(8.13 - 1.6518\sigma_1 + 0.5506\sigma_1^2). \qquad 2)$$

The curve by Eq.2 can represent well the measured E_L within the estimated applied stress range, from σ_1^0 to σ_1^a. The averaged modulus, E_L^* in this range can be calculated by the following formula[9]:

$$E_L^* = [\mathrm{atan}\{(\sigma_1^a+B)/A\} - \mathrm{atan}\{(\sigma_1^0+B)/A\}] / \{3A\, S_{1111}\, (\sigma_1^a - \sigma_1^0)\} \qquad 3)$$

where $A = \{ \frac{1}{3} (S_{11}/S_{1111}) - B^2 \}^{1/2}$ and

$$B = \frac{1}{3} (S_{111}/S_{1111}) . \qquad 4)$$

Thus, we have $E_L^* = 117.3$ GPa, in the range from 0 to 460MPa in the buckling tests. This E_L^* is adopted in eigenvalue analysis instead of purely nonlinear analysis with variable moduli. The supposed V_f is 60% for APC-2. As other independent orthotropic elastic constants, the following experimental value in Ref.13 are used:

$$E_T=10.3\mathrm{GPa}, G_{LT}=4.62\mathrm{GPa}, \nu_L=0.38, G_{TT}=3.43\mathrm{GPa}. \qquad 5)$$

The transverse shear modulus G_{TT} is obtained by the assumptions of transverse isotropy and $\nu_{TT}=0.5$.

Some comments about finite element analysis is given below. A selected element is a laminated composite shell available in NISA-II which is geometrically a quadrilateral with 8 node. This element can take the transverse shear effect into account[15]. A convergence property is checked individually for stiffeners and skins. A mesh pattern used for the panel part is shown in Fig.20. The coordinate system is taken so that the y axis coincides with the loading direction and that the xy plane does the skin surface. Hence, 0° lamina is parallel to

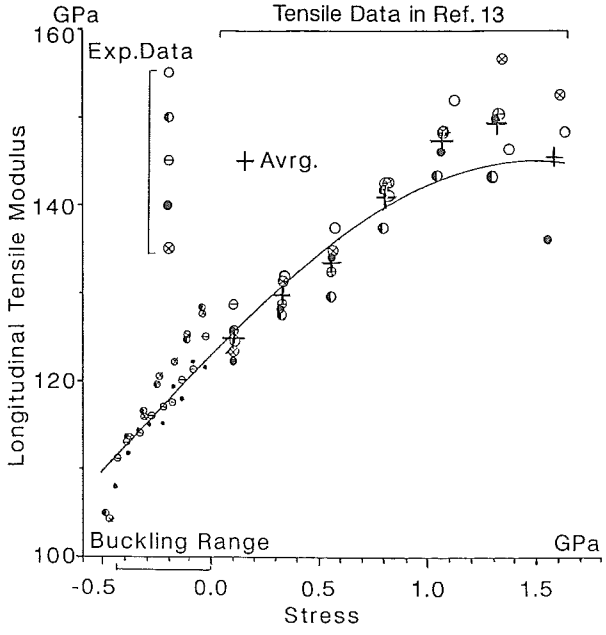

Figure 19 Dependency of Longitudinal Elastic Modulus on Stress in Unidirectional CFRP

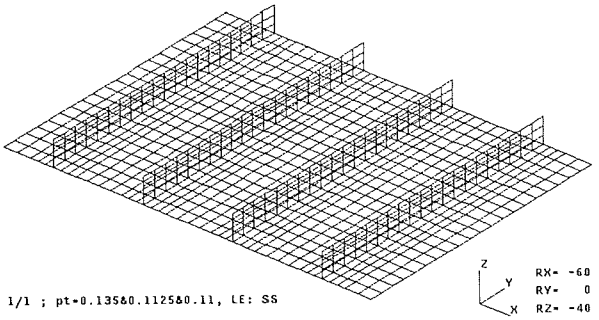

Figure 20 FEA Mesh Pattern for CFRP Panel Portion

the y direction. Aluminum end fixtures 24mm thick and potting material of epoxy resin type, EA934, in 10mm groove are sometimes included into the FEA. A 3-D brick element composed of 8 or 6 nodes is employed with the shell element in such cases. An illustration around the fixture is shown in Fig.21. Note that a length between fixtures, a net length of the panel, and a total length of the specimen is 260, 280, and 308mm, respectively.

5.2 EFFECT OF LONGITUDINAL MODULUS

In order to clarify the effect of the input elastic moduli, calculations are performed with the present set of elastic moduli, the sets of Ref.8, of Ref.10 and of Ref.11 for the present model geometry of the latest CF/PEEK panels, denoted as PEH. The results are indicated in Fig.22. The other model parameters are as follows: Length ℓ is 280mm, model size is 1/4 without the end fixture, loading edge boundary condition is simply supported, and assumed t_p = 0.11 and 0.1125. Later explanation should be referred for the detail of these parameters. Note that this set of the parameters is chosen only due to shorter CPU time and that it never means the best correlated case.

Figure 22 clearly demonstrates that the set of elastic moduli in Ref.8 provides the highest prediction among the present cases. Although there can be found some relatively wider variety in E_T, G_{LT}, and ν_L than E_L among the sets in Refs. 10, 11 and the present case such as the present E_T 45% larger than the value in Ref.11, E_L seems to be more predominant factor for the predictions. Normalized plots of buckling stresses to E_L shown in Fig.22 endorse this idea. In summary, E_L plays a crucial role in the prediction of buckling stresses.

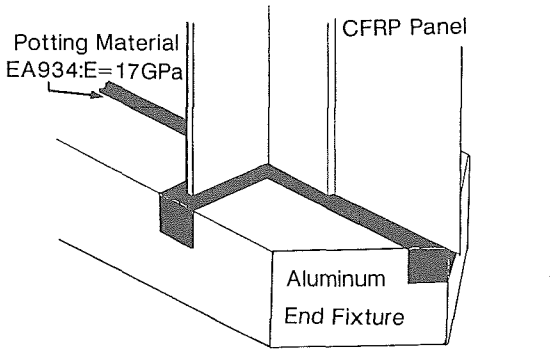

Figure 21 Illustration around Potting and Metal End Fixture

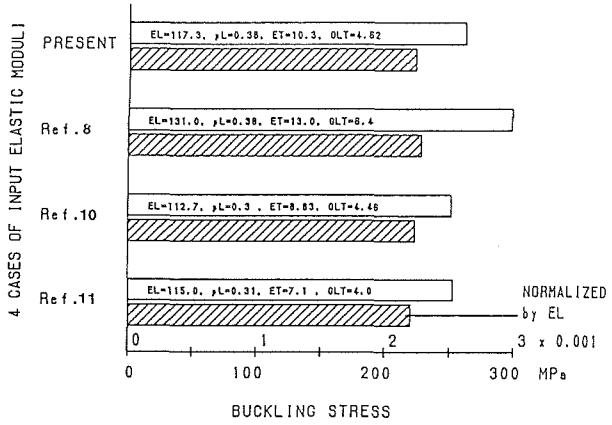

Figure 22 Influence of Input Elastic Moduli upon Buckling Stress (1/4 Model without Fixture, ℓ=280mm)

5.3 EFFECT OF MODEL GEOMETRY

Boundary conditions on loading edges are very important in buckling problems generally. In the present panels, sensitivity in the numerical prediction related to them could be expected because of a shorter geometry than the other experiments. Some calculations are performed in order to clarify this point. The current model geometry and the stacking sequence of PEH is assumed here and so are the set of moduli of E_L^* = 117.3 GPa and the values of Eq.5, and t_p = 0.11 and 0.1125.

A summarizing plot to the present question is indicated in Fig.23. Legends of 1/1 and 1/4 signify the modelled region of the panel in FEA. Conditions of the symmetry are assumed along the center lines in the latter case. They are not satisfied in the most rigorous sense due to the nature of the rotational symmetry of the laminate. Thus, examination of such a quarter model will be discussed later. In the cases without end fixture, simply supported conditions are assumed along the loading edges of the skin, whereas the deflection in the x direction

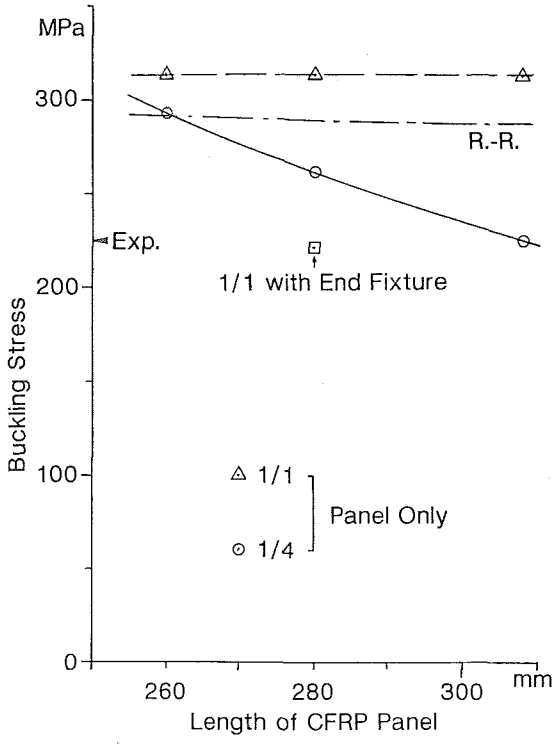

Figure 23 Relationships between Panel Geometry, FE-Modelling and Buckling Stress

is assumed to be zero along the loading edges of stiffeners. The model length is fictitiously changed from 260mm to 308mm. Note that the length is doubled for plotting in the 1/4 cases. The results for the panel only show poor agreement with the experimental value of the PEH panels. Although the demonstration of the buckling modes is omitted here, neither of 1/1 nor 1/4 models by panel only is correlated well with an experimental buckling mode for PEH-01 shown in Fig.24 by a Moire-topography camera at 269MPa. The picture indicates that mid-bay skins buckle with one half wavelength in both x and y directions. Measured deflections in Fig.18 are consistent with this picture.

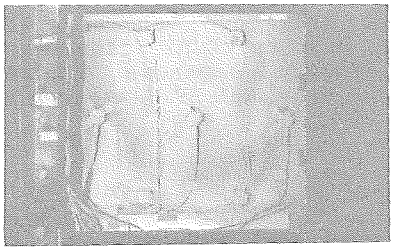

Figure 24 Moire-Topography Picture for Buckling Mode of PEH-01 Panel (PEH-01) at 269MPa (Buckled at 220MPa)

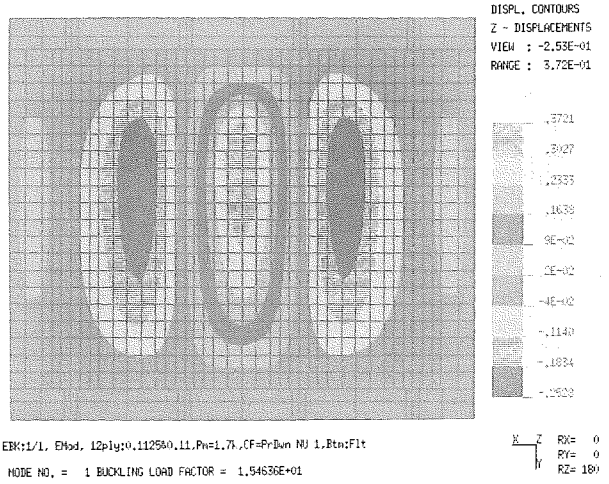

Figure 25 Out-of-Plane Deflection Contour for 1/1 Model with End Fixture Based on PEH Properties

According to the above findings, FEA based on the models with the end fixture are performed where the compression force is idealized as distributed pressure. The employed model parameters are as follows: Present set of CFRP moduli, 72.6GPa and 17 GPa as fixture and potting material moduli, and ply thickness of 0.11 and 0.1125. The 1/1 result, 221.6 MPa, is plotted in Fig.23 by an open square which coincides with the experimental average excellently. For the comparison of buckling mode, an isovalue contour and a line plot of the out-of-plane deformation of the 1/1 result are depicted in Figs. 25 and 26, respectively. The mode indicated is fairly similar to the experimental one in Fig.24 except for the position of deflection peak. Thus, a consideration of the end

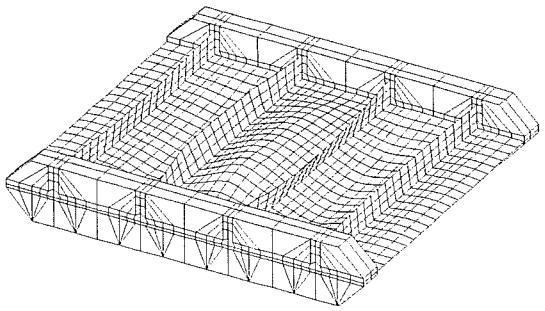

Figure 26 Buckling Mode by 1/1 Model with End Fixture

fixture is a very crucial point for a better correlation in the case of shorter stiffened panels. However, this model requires roughly 9900 DOF and is regarded as non-economical.

For the nonlinear analysis, a reduced model providing reasonable results is strongly desired. A 1/4 model of 2450DOF with the fixture is chosen for this purpose and its result of buckling stress is 221.2MPa for the same model parameters as the 1/1. The difference in buckling stresses of the 1/1 and 1/4 regions is only 0.2%. The main feature of the buckling mode of a half wavelength in a mid-bay skin is maintained. Thus, this model can be considered as the irreducible minimum in the current problem.

5.4 EFFECT OF INITIAL IMPERFECTION

Initial imperfection is basically important in general buckling problems. Because little information about the effect of initial imperfection of composite stiffened panels is available, some parametric studies are conducted here. Due to mismatch of coefficients of thermal expansion, a free shape of the present CF/PEEK panel as fabricated looks roughly like a segment of a cylindrical shell as shown in Fig.27. During a potting process, it is globally straightened up whereas some local waviness occurs. Two types of initial imperfection shape functions, $w_i(x,y)$ are assumed: Single curvature composed of sine wave in the x direction with the wavelength of the distance between stiffeners and double curvature composed of a product of the same function in the x direction and a sine wave in the y direction with the half wavelength of the distance between the fixtures. In both cases, w_i is assumed to be zero along the unloaded side edges. The maximum amplitude of these functions is considered as a representing parameter.

Figure 27 demonstrates the effect of the present types of initial imperfection. It is observed that negative $W_{i\,max}$ which is convex toward skins provides higher buckling stress in both imperfection functions. Such tendency is physically reasonable due to smaller off-neutral distance. In other words, stiffeners carry

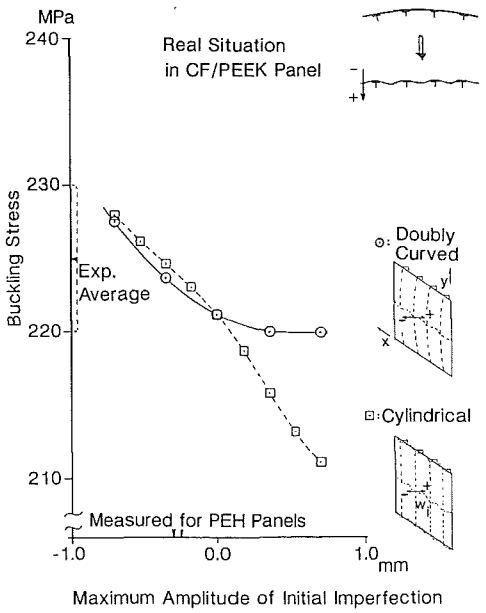

Figure 27 Effect of Initial Imperfection upon Buckling Stress: FEA for CF/PEEK, 1/4 models with End Fixture

little more load in the cases with negative $W_{i\,max}$. The measured mean values of $W_{i\,max}$ for two PEH panels are about -0.3 mm. Thus, a consideration of a realistic initial imperfection leads to more better correlation between numerical prediction and experiments.

A description about a simple Rayleigh-Ritz method is omitted. Reference 4 should be consulted for detail. Also, exhibition of nonlinear results are skipped.

6. CONCLUSIONS

Experimental and numerical investigation is conducted for CAI properties of stiffened panels of CF/PEEK and CF/Epoxy. Linear relationship of delamination areas to applied impact energy is clarified for CF/PEEK in contrast with CF/Epoxy. Impacts on skin degrade almost nothing of CAI properties while those on stiffeners affect them considerably. The process of delamination buckling in panel CAI tests is well understood. Onset of delamination propagation in CF/Epoxy panels is well related to the critical CAI strain of flat thick plates of the same material. Because of structural fail-safe property of stiffened panels, reduction of CAI strengths in CF/Epoxy is not so serious as flat plate cases. Due to an ability of delamination arresting, CAI strengths of CF/PEEK panels are quite high.

Numerical analysis and its rigorous correlation with experiments reveal the following findings. Decreasing longitudinal elastic modulus of UD CFRP lamina in compression plays a crucial role for better numerical predictions of buckling stress. A consideration of the elastic constraint by the end fixtures plays another key role for the present short panels. A quarter model with the fixture provides a good compromise between accuracy and economy. A realistic shape and amplitude of initial imperfection increases the buckling stress a little and leads to a better agreement with the experiment.

ACKNOWLEDGEMENTS

The authors gratefully acknowledge the skill and expertise of people of Fuji Heavy Industries (FHI) Inc. in the fabrication of stiffened panels of CF/PEEK. They also wish to thank Science and Technology Agency of Japanese Government for their funding of NAL SP. Research Program.

REFERENCES

1. J. H. Starnes, Jr., M. D. Rhodes and J. G. Williams, ASTM STP 696, R. B. Pipes, Ed., ASTM, 1979, pp. 145-171.
2. T. Ishikawa, Y. Noguchi and M. Matsushima, J. of Japan Society of Composite Materials, 13, (2), 63 (1987), (in Japanese).
3. DATA Sheet 3a;Property Data of APC-2, Fiberite, Laguna Hill, CA, 1987.
4. T. Ishikawa, M. Matsushima, Y. Hayashi and T. Noguchi, Proc. of 5th Japan US. Conf. on Composite Materials, June 1990, pp. 445-452.
5. NASA, "Standard Tests for Toughened Resin Composites :Revised Edition," NASA RP 1092, July 1983.
6. J. E. McCarty and R. E. Horton, Proc. of 15th Congress, International Council of Aero. Sci., London, England, Sept. 1986, Handout Paper.
7. K. Ono and Y. Tada, Proc. of 26th Structural Conference of Japan Soc. Aeronautical and Space Sciences, July 1984, pp. 352-355, (in Japanese).
8. J. H. Starnes, Jr., N. F. Knight, Jr. and M. Rouse, AIAA J., Vol.23, No.8, Aug. 1985, pp. 1236-1246.
9. S. M. Causbie and P. A. Lagace, Proc. of AIAA 27th Structures, Str. Dyn. Mat. Conf., Part 1, May 1986, pp. 280-287.
10. S. Sanbongi, S. Toda, and E. Nakai, J. of Japan Society of Aero. & Space Sci., Vol.30, No.338, Mar. 1987, pp. 127-133, (in Japanese).
11. J. F. M. Wiggenraad, Proc. of 5th Int. Conf. on Composite Materials, TMS-AIME, San Diego CA, USA, July 1985, pp. 1377-1392.
12. D. Bushnell, Computers & Structures, Vol.25, No.4, 1987, pp.469-605.
13. T. Ishikawa, M. Matsushima, and Y. Hayashi, J. of Materials Science, Vol. 20, 1985, pp. 4075-4083.
14. T. Ishikawa, M. Matsushima, and Y. Hayashi, to appear.
15. Engineering Mechanics Research Corporation: Users Manual of NISA-II, Version 91, Apr.1991.